

Multi-View 3D Instance Segmentation of Structural Anomalies for Enhanced Structural Inspection of Concrete Bridges

Christian Benz^{1a}, Volker Rodehorst^a

^aComputer Vision in Engineering, Bauhaus-Universität, Schwanseestraße 143, Weimar, 99427, Thuringia, Germany

Abstract

For effective structural damage assessment, the instances of damages need to be localized in the world of a 3D model. Due to a lack of data, the detection of structural anomalies can currently not be directly learned and performed in 3D space. In this work, a three-stage approach is presented, which uses the good performance of detection models on image level to segment instances of anomalies in the 3D space. In the *detection stage*, semantic segmentation predictions are produced on image level. The *mapping stage* transfers the image-level prediction onto the respective point cloud. In the *extraction stage*, 3D anomaly instances are extracted from the segmented point cloud. Cloud contraction is used to transform cracks into their medial axis representation. For areal anomalies the bounding polygon is extracted by means of alpha shapes. The approach covers the classes *crack*, *spalling*, and *corrosion* and the three image-level segmentation models TopoCrack [1], nnU-Net [2], and DetectionHMA [3] are compared. Granted a localization tolerance of 4 cm, IoUs of over 90% can be achieved for crack and corrosion and 41% for spalling, which appears to be a specifically challenging class. Detection on instance-level measured in AP₅₀ is about 45% for crack and spalling and 73% for corrosion.

Keywords: Structural Condition Assessment, Structural Inspection, Structural Health Monitoring (SHM), Deep Learning, Crack Detection, 3D Anomaly Detection

1. Introduction

The importance of structural health monitoring (SHM) for modern societies is undisputable. It ensures critical infrastructure to stay operational or to be, if necessary, renewed in a timely and systematic manner. Thereby, it contributes to the safe and enduring usage of critical infrastructure, a crucial component in the functioning of modern societies. Transportation routes rely on infrastructure to enable good's delivery and individual mobility. In particular, bridges are used to shorten routes or bypass rough terrain, which sometimes renders them the only viable connection between two locations. The exposure to weathering and diverse forces makes bridges especially vulnerable to degradation and unforeseeable collapse often has catastrophic dimensions. The regular inspection of bridges is, thus, of high societal benefit, while posing substantial challenges for men and machines involved.

The availability and utilization of new technologies has led to a growth of research activity on automating structure inspection. Especially, the advent of more versatile image acquisition platforms, such as UAS (unmanned aircraft system, aka drones), and advanced data algorithms, such as machine learning, have boosted research and engineering in the field. With ever more and better technologies and data at hand, the gap to real-world application is gradually about to close.

As a consequence, research on the image-based recognition of structural anomalies on the surface of critical infrastructure

is rapidly growing. While current work focuses on detecting cracks and other anomalies on image level, the transfer of this information into the 3D space of point clouds is underexplored. The severity of an anomaly, however, substantially depends on the place of its occurrence on the structure. The proper location of an anomaly on the structure is hardly accessible with reference to the images alone. Thus, the extension of the detection of structural anomalies beyond the image level forms the subject of this work.

For effective structure inspection in 3D, the transfer of detection results from image level to the 3D space is one key aspect. However, only the discretization of mapped results into dedicated anomaly instances in 3D enables the quantitative analysis of their extend. Information such as the length and width of cracks or the area covered by corrosion or spalling can sustainably support the decision process of the experts involved. Furthermore, it paves the road for improved traceability, objectivity, and verifiability of the inspection criteria that determine particular decisions.

For that purpose, a workflow is here presented, that accomplishes the segmentation of instances on a 3D point cloud. It makes use of SOTA models for semantic segmentation of structural anomalies on image-level (*detection stage*) and projects the 2D predictions on a 3D point cloud (*mapping stage*) by means of point colorization. This procedure does not yield anomaly instances. Thus, the points are subsequently clustered and cracks are transformed into medial axes while bounding polygons are used to represent areal anomalies (*extraction stage*). The obtained anomaly instances enable the computation

¹Corresponding author, christian.benz@uni-weimar.de

of additional quantitative indicators such as the crack width and length or the area and circumference of areal anomalies.

The main contributions of this work are:

- The demonstration and implementation of a fully-functional workflow for the detection, mapping, and extraction of structural anomalies in 3D point clouds.
- The introduction and application of reasonable transformations of cracks and areal anomalies into measurable 3D instances.
- A thorough evaluation and comparison of SOTA models for the proposed workflow of 3D anomaly instance segmentation on real-world data.

After the presentation of the related work, the detection workflow is explained in-depth encompassing the detection, mapping, and extraction stage. Extensive evaluation demonstrate the strengths and weaknesses of the approaches and visualizations provided a qualitative impression of the results.

2. Related Work

Three major fields of related work are identified: the detection of cracks and other structural anomalies on image level as well as approaches to 3D anomaly detection.

2.1. Crack Segmentation

[4] provide a survey on crack detection before artificial neural networks (ANN) became the dominant approach. Edge detection, morphological operations, filtering, and thresholding were among the most frequently used techniques [5, 6, 7, 8, 9, 10, 11]. The CrackTree approach [12] constructs a minimum spanning tree over previously identified crack seeds. An ensemble of decision trees called CrackForest is used by [13] for crack classification.

Since 2017, artificial neural networks (ANN) have emerged as the dominant approach for crack detection. [14] conducted a study comparing different training configurations of AlexNet [15] with six edge detectors, including Sobel, LoG, and Butterworth. Experiments on the SDNET dataset [16] indicated the superiority of ANN and the effectiveness of transfer learning. Other approaches, proposed by [17, 18, 19], involve using a classification CNN combined with a sliding window to process larger images and/or improve localization. [20] popularized the transition to fully-convolutional networks (FCN) [21] for crack segmentation. Based on SegNet [22], DeepCrackZ was designed [23]: a separate fusion logic with individual, scale-wise losses supports preserving thin structures. The conceptually similar approach DeepCrackL² is suggested by [24]. In the style of deeply-supervised nets (DSN) [25], losses are computed for intermediate side-outputs to make use of fine details and anti-noise capabilities alike. The outputs undergo

²DeepCrackZ and DeepCrackL are used for disambiguation since both were originally named ‘DeepCrack’.

post-processing with guided filtering (GF) [26] and conditional random fields (CRF) [27]. A U-Net [28] with focal loss [29] is reported to perform superiorly compared to a simpler FCN design [30]. [31] propose the feature pyramid and hierarchical boosting network (FPHBN). It extends holistically-nested edge detection (HED) [32] by a feature pyramid module to incorporate and propagate context information to lower levels. The hierarchical boosting supports the inter-level communication within the FPHBN. [33] develop CrackFormer, which is a transformer-based approach to crack segmentation. For that purpose, the convolutional layers of VGG [34] are replaced by a self-attention logic. To increase the crack sharpness, a scaling-attention block is suggested. [3] propose a re-trained version of the hierarchical multi-scale attention network by [35] called HMA, which mitigates the scale sensitivity of cracks. The results are aggregated based on the attention to cracks on different levels of scales. In order to preserve the continuity of cracks, [1] suggest TOPO loss, which uses maximin paths to mitigate discontinuities between cracks. An oriented bounding box approach, named CrackDet, has recently been proposed by [36]. [37] and [38] emphasize the usefulness of transfer learning and compose smaller crack datasets into larger ones, Conglo, and CrackSeg9k. [38] compare a number of approaches, including Pix2Pix, SWIN, and MaskRCNN. DeepLabV3+ [39] with a ResNet-101 backbone outperformed the other methods. [37] confirm that DeepLabV3+ is an effective method for crack segmentation.

2.2. Detection of Structural Anomalies

While a multitude of datasets and approaches on crack detection has been published over the past years, interest and resources on the image-based detection of other structural anomalies has only recently picked up pace. Analogous to crack detection, the paradigm of image classification to anomaly detection was first explored. Classes such as spalling and efflorescence are featured by the CODEBRIM [40] and MCDS [41] datasets. A meta-learning approach for neural architecture search (NAS) on CODEBRIM is proposed by [40], which slightly outperforms VGG- [34] and DenseNet-based [42] approaches. The NAS-based model requires distinctly fewer parameters. Benchmarking and extensive hyperparameter tuning for transfer learning on these datasets is performed by [43].

Science 2021, a shift towards semantic segmentation for structural anomaly detection has been observed. [3] published the S2DS dataset with 743 images, which features anomalies such as crack, spalling, corrosion, efflorescence, and vegetation. The proposed DetectionHMA [3] uses attention maps over different scales to effectively exploit multi-scale information. To systematize the increasing number of datasets, [44] surveyed published datasets for structural inspection and started an initiative to list available datasets³. The CSSC [45] dataset represent cracks and spalling. CrSpEE [46] covers the same anomalies in an ‘in the wild’ scenario, i.e. with substantial distractors (people, context, background) being present. Very recently [47]

³https://github.com/beric7/structural_inspection_main/tree/main/cataloged_review, accessed 29 Dec, 2023.

published the dacl10k dataset which contains 10,000 images and i.a. includes the classes crack, spalling, rust, efflorescence, wetspot, rockpocket, and weathering. The corresponding challenge hosted at WACV'24 [48] indicated the power of transfer learning on SOTA models for semantic segmentation such as ConvNeXt-Large [49], EVA-02-Large [50], or Mask2Former [51] and the extensive usage of ensembles.

2.3. 3D Anomaly Detection

The attention in the image-based detection of cracks and other structural anomalies in the 3D space has recently been growing. The state is premature and a lack of publicly available datasets is observed that interferes with effective model training and evaluation. For 3D anomaly detection in the industrial context, the MVTec 3D-AD dataset was published [52]. The dataset features point clouds with scratches, holes, deformations, and other anomalies in ten industrially relevant categories, including cookies, carrots, dowels, and ropes. For MVTec 3D-AD, [53] transfer an unsupervised student-teacher approach to 3D and infer defective point clouds from deep feature descriptors. The application context of MVTec 3D-AD differs from structural inspection by the controlled acquisition circumstances, the achieved 3D resolution, and the captured objects.

Over the last decade, a number of approaches specifically have targeted 3D structural inspection. [54] propose a system for 3D crack detection by combining the information from multiple images making use of the depth information obtained from SfM. To spot cracks in a triangulated mesh, [55] make use of the deviation of normals compared to the medial axis of an element. [56] use depth information captured by a laser scanner to support image-based crack segmentation. A CNN named CrackNet is presented by [57], which operates on depth maps for pavement cracks. A learning-based successor is proposed by [58]. Embedding features for 3D points are extracted by [59] and used to segment crack regions in an unsupervised manner. [60] pre-segment building facades and subsequently project cracks, that were segmented on image level, onto the 3D model.

Based on the comparatively low resolution of point clouds in real inspection scenarios, methods operating natively on point cloud level render suitable for the application case of this work. 3D anomaly detection is, thus, here approached by using the higher resolution from multiple views. Since data are currently too scarce, end-to-end training of a multi-view point cloud segmentation method is currently not feasible. Therefore, the effective performance of anomaly detection in 2D is leveraged in a multi-stage approach to effectively transform 2D results into 3D anomaly instances.

3. Data

Due to the recency of the field, no proper, labeled 3D data for structural anomaly detection is yet available to the public. Reasons for the absence of such datasets include:

Reachability: Many parts of structures are typically not reachable without greater effort. Modern image acquisition platforms such as UAS facilitate reachability, which, however, remains a challenging endeavor.

Region of Interest: The surface of structures is large and anomalies typically occur rare and punctually. The identification of relevant regions is a labor-intensive task. In that respect, it must be considered a hen's egg problem: the goal of 3D anomaly detection is to automate this process. Dataset creation, however, first requires the manual retrieval of anomalies.

Quality Requirements: Crack detection poses challenging requirements in terms of image resolution. Acquiring overlapping images of resolution 0.15 mm with good quality by means of a moving platform (such as UAS) is a distinct challenge leading to only a few usable datasets of respective quality and resolution.

Labeling Effort: Effective labeling must include field experts, which are rarely available (or willing) for labeling data in a wider scope.

Scalability: Point clouds scale weakly for very high resolutions leading to point clouds of more than 20M points. Therefore, technical reasons currently call for point clouds of manageable size.

Data Protection: The structure maintainers do usually not want the (potentially defective) structure to be exposed to the public. Beside bringing negative publicity, the defectiveness of a structure could also be exploited for (terrorist) attacks.

3D Structure: Usually, a large portion of a structure's surface is planar. Only few parts exhibit non-planar areas such as corners or niches. Exploring 3D anomaly detection renders reasonable only on defective non-planar parts of the structure.

Despite the listed obstacles, a dataset was created in the context of this work. The dataset features four segments from two concrete bridges that showed anomalies suitable for 3D anomaly detection.

3.1. 3D Reconstruction

Capturing 3D real-world data is a challenging task, which is typically performed by processing 2D representations and thereupon inferring the 3D Structure. While a number of methods for measuring the 3D structure of objects are available – including *structured light sensors* and *time-of-flight* (TOF) cameras (e.g. [61]) – image-based stereo reconstruction is the standard procedure in structural inspection.

The reconstruction of a static 3D scene from multiple images still follows the principles published in [62]: The *structure-from-motion* (SfM) pipeline infers the relative orientation of the views, which is subsequently used to perform *multi-view stereo* (MVS) yielding a dense point cloud. This procedure

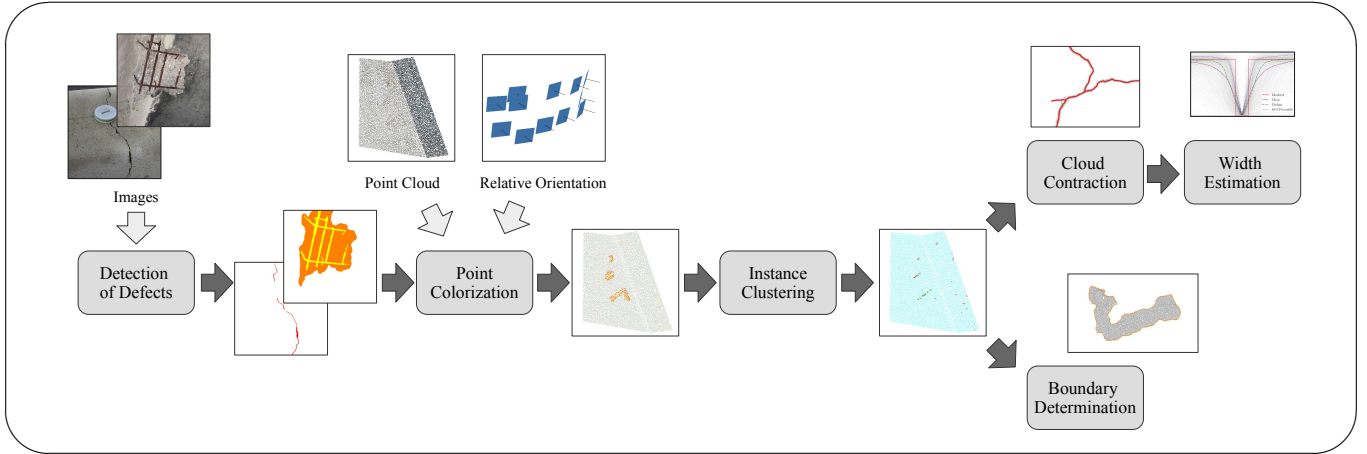


Figure 1: Components and workflow of the 3D detection pipeline.

	Bridge B		Bridge G	
	Dev	Test	Dev	Test
Points	26.5 M	22.7 M	23.2 M	36.0 M
Resolution [$\frac{\text{mm}^2}{\text{pt}}$]	0.026	0.027	0.172	0.219
Views	20	22	28	16
Anomaly Instances				
Cracks	37	20	–	–
Spalling	–	–	9	8
Corrosion	–	–	8	13

Table 1: Dataset for 3D anomaly detection in a real-world inspection scenario split into a development and test sets. Two bridges with two segments each are featured showing anomalies such as cracks, spalling, and corrosion.

is implemented in the COLMAP⁴ software [63, 64], widely used in academia and industry. Beside COLMAP, which is available under a permissive open-source license, a number of commercial products exists such as Reality Capture⁵ or Agisoft Metashape⁶. The latter of which was used in this work to compute a 3D point cloud and textured mesh from the captured images.

3.2. Dataset

Table 1 provides an overview of the created dataset. Bridge B is a highway bridge in Germany, that shows comparatively wide cracks in the range of 0.5 to 1.0 mm. One of the bridge’s accessible piers was captured with a Sony $\alpha 7r$ I camera being moved around the pier’s base on a tripod adjusted to two different altitudes. The second object, Bridge G, is a railway bridge showing defects of spalling and corrosion. The images were captured by means of the UAS, Intel Falcon 8+, with a Sony $\alpha 7r$ I camera being mounted on a compatible gimbal. Four segments were extracted from the two bridges, which showed relevant anomalies at niches or corners. One segment of each bridge is used

in the development set for parameter tuning, the other two segments form the test set. For a visual impression of the two test segments, please refer to Figure 4.

3.3. Annotation Protocol

In practical scenarios, the resolution of the reconstructed dense point cloud is typically lower than the resolution on image-level. Thus, the accurate annotation of cracks and anomaly boundaries on the dense cloud rendered infeasible. Due to the local planarity of the surface, a triangulated mesh could be reconstructed and a high-resolution texture was computed. The texture forms an adjusted mosaic of the respective images, approximating the image-level resolution. Polylines for cracks and polygons for corrosion and spalling were annotated using the polyline tracing function provided by CloudCompare⁷.

4. Workflow

Figure 1 schematically depicts the components of the proposed workflow to transform the 2D information into 3D anomaly instances. It is assumed, that 3D reconstruction as described in Section 3.1 was successfully performed beforehand. The three major stages are the (1) the *detection stage* (“Detection of Defects”), the (2) *mapping stage* (“Point Colorization”) and the (3) *extraction stage* (“Instance Clustering”, “Cloud Contraction”, “Boundary Determination”, and “Width Estimation”). In the *detection stage*, a model for semantic segmentation is run on all images, returning class probabilities for all pixels of the input image. The *mapping stage* transfers these 2D class probabilities to the dense cloud yielding a semantically segmented point cloud. In the final *extraction stage*, the segmented point cloud is clustered and the respective subclouds are transformed into anomaly instances. For crack instances the crack width is subsequently estimated.

⁴<https://colmap.github.io/>, accessed Dec 20, 2023.

⁵<https://www.capturingreality.com/>, accessed Dec 20, 2023.

⁶<https://www.agisoft.com/>, accessed Dec 20, 2023.

⁷<https://www.danielgm.net/cc/>, accessed Dec 29, 2023.

5. Detection Stage

For the detection on image level, off-the-shelf models for anomaly segmentation can be applied. The color images obtained e.g., by means of UAS, mobile phones, or hand cameras are processed by a segmentation model, which returns probability maps (also referred to as *heatmaps*) for each of the classes under investigation (*crack, spalling, corrosion, and background*). In this work, the three SOTA approaches TopoCrack [1], nnU-Net [65], and DetectionHMA [3] are used and compared. All of which are based on convolutional neural networks (CNN), a specific kind of artificial neural networks.

TopoCrack. With the goal of preserving the crack continuity, [1] introduce a novel topological loss called *TOPO loss* and benchmark it against other losses. The base architecture is formed by TeraNet [66], which is a U-Net-based architecture with VGG11 encoder. Beside the dice loss, MSE for distance regression and TOPO loss for topology preservation are explored. Distance regression is based on truncated distance maps which are inferred from the segmentation labels. Each pixel in the distance map represents the distance to the closest crack. Distances over 20 pixels are truncated. The truncated distance maps are used with MSE loss to enforce the model to learn the correct distances to the closest crack. Based on [67] TOPO loss uses the concept of a maximin path. The maximin path is the path of minimal length connecting two pixels with the maximum values gathered along the way. In this context, the values are drawn from the distance map. For a continuous crack, the maximin paths that connect the background regions left and right of the crack contain a zero value, which is the crossing of the crack center. Maximin paths with values larger than zero indicate a discontinuity in the crack and are, thus, penalized. The combination of MSE and TOPO loss is reported to have an F_1 score of 69% on the alongside published dataset.

nnU-Net. The nnU-Net approach was proposed by [65] and published in Nature Methods in 2021. Ranking first in the majority of MICCAI⁸ challenges in 2020 and 2021, nnU-Net attracted major attention in the field of medical imaging. An extended version of nnU-Net also won the AMOS challenge on abdominal multi-organ segmentation in 2022 [68]. The main benefits of nnU-Net are the minimum of manual intervention required for designing a model and the applicability on 2D and 3D segmentation tasks alike. [2] indicate the usefulness of nnU-Net beyond the medical domain for 2D semantic segmentation of structural defects.

The term nnU-Net refers to ‘no new net’ since it does not propose any new network architecture, loss function, or training scheme [65]. It rather systemizes the process of ‘methods configuration’ and delegates it to a set of fixed, rule-based, and

⁸MICCAI stands for *Medical Image Computing and Computer Assisted Interventions* and refers to the highest-ranked annual computer science conference in the domain of medical imaging (ranking according to <https://research.com/conference-rankings/computer-science>, accessed on August 31, 2023). The conference is hosted by the MICCAI society <http://www.miccai.org/>.

empirical parameters for automated self-configuration. Based on the *data fingerprint* inferred from the particular dataset, heuristic rules guide the *rule-based parameters* of data handling (such as resampling strategies, intensity normalization, patch and batch sizes) and the adjustment of the architecture template. The training is based on *fixed parameters* with respect to the optimizer, learning rate, data augmentation, and loss function and runs in a scheme of 5-fold *cross validation*. In 5-fold cross-validation for each fold 20% of the training set is left out for validation purposes. 5-fold cross-validation eventually yields five models of the same architecture but different parameters. In a post-processing step an *ensemble* is empirically determined which combines the results of the five models. The architecture template of nnU-Net is based on the widely used U-Net design principle [28]. nnU-Net was trained on the S2DS dataset (see below).

DetectionHMA. DetectionHMA⁹ is proposed by [3] for detecting structural defects on concrete surfaces. It is based on hierarchical multi-scale attention approach by [35], by the time a top performer with available code on the cityscapes benchmark [69]. To overcome scale-invariance regularly observed for CNNs, HMA incorporate multiple scales and proposes a dynamic combination of results from different scales based on simultaneously generated attention maps. The attention maps are contrastively learned based on two scales only. For inference, however, the number of scales can be arbitrarily chosen. For DetectionHMA the scales 1.0, 0.5, and 0.25 rendered useful. As a backbone, HMA uses the HRNet-OCR [70], where OCR refers to object-contextual representations. The object-contextual representations are used to augment the pixel’s representation with contextual information. HMA uses the *region mutual information (RMI)* loss introduced by [71], which combines a cross-entropy component with a component representing mutual information.

DetectionHMA was trained on the S2DS (structural defect dataset) dataset, consisting of 743 images [3]. The dataset contains images from real inspection sites taken by various camera types and features the classes background, crack, spalling, corrosion, efflorescence, vegetation, and control point. Due to lack of 3D data for other classes, this works is confined to crack, spalling, corrosion, and background.

6. Mapping Stage

In the mapping stage, the results on image level are mapped into 3D space. More specifically, the probability information given in the 2D heatmaps are transferred onto the 3D point cloud. For that purpose, *point colorization* is performed with class labels acting as the respective colors. The points are projected into all views and the gathered information are aggregated into a single class label for each 3D point. This procedure is performed in parallel on batches of points of the point cloud.

⁹<https://github.com/ben-z-original/detectionhma>, accessed Dec 29, 2023.

The information aggregation from the views follows a fusion logic. It is assumed, that views more perpendicular to a point are supposed to contribute a higher degree to a point's class than views from oblique directions. The deviation between view and point is measured by the angular difference between the point's normal and the viewing direction. The information is aggregated by the following weighting scheme:

$$w_i = \begin{cases} \frac{1}{N}, & \text{if } 130^\circ < \theta < 230^\circ \\ 0, & \text{else} \end{cases} \quad (1)$$

The term w_i refers to the weight for view i for a certain point of the dense point cloud. N denotes the number of views the point is visible in. The view is only considered in case the angular deviation θ between the viewing direction and the point normal is in the range $(130^\circ, 230^\circ)$. The weighting is performed on each class channel individually. Subsequently, a class label is assigned to the point based on a winner-takes-all logic, i.e. the class with the highest value is assigned and the others are discarded.

7. Extraction Stage

The result of the mapping stage is a point cloud, in which each point was assigned a certain class label. The classes considered in this work are *crack*, *spalling*, *corrosion*, and *background*. A point cloud is a set of independent points which per se do not have further knowledge about their neighborhood. Thus, it is unclear, if points of the same class do actually represent the same or different instances of a defect. For advanced quantitative analyses it is, however, essential to extract discrete instances of anomalies.

7.1. Clustering

It is assumed, that points of equal class and sufficient proximity represent the same instance of a defect. This assumption holds for crack, spalling, and corrosion alike. The *density-based spatial clustering of applications with noise* (DBSCAN) [72] algorithm groups points based on their distance. A specified minimal number of points within a certain distance forms a local high-density neighborhood which represents a cluster. Low-density neighborhoods are considered noise and consequently discarded.

The point cloud is split into three subclouds, one containing all crack points, one containing all spalling points, and one containing all corrosion points. All background points are discarded. DBSCAN runs on all subclouds and assigns a cluster ID to each point. Consequently, each point has information about which instance of a defect it represents. Due to their line-like character, cracks undergo different further processing than spalling and corrosion.

7.2. Cracks

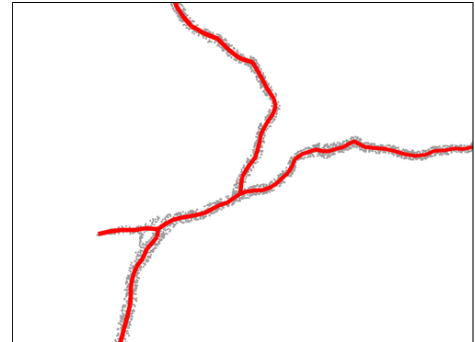
The point cloud representation is not suited for quantitative analyses of the detected cracks such as determining the length, number of branches, or the direction of propagation. For that



(a) Textured mesh with crack.



(b) Clustered subcloud of crack.



(c) Contracted medial axis.



(d) Medial axis on textured mesh.

Figure 2: Illustration of the cloud contraction for extracting the medial axis of a branching crack: (a) shows a mesh with high-resolution texture, (b) the subcloud after clustering, (c) the overlaid medial axis (red) obtained by cloud contraction, and (d) the medial axis overlaid over the textured mesh.

purpose, the clustered point cloud is transformed into a polyline representation referred to as (curve) skeleton or *medial axis*. Despite slight differences, the terms (curve) skeleton and medial axis are used interchangeably in this work. Figures 2a to 2d illustrate the stages of crack extraction.

Figure 2a shows the crack on a mesh with high-quality texture. By means of clustering, a subcloud is obtained which represents the specific instance of the crack, Figure 2b. For extracting the medial axis of the subcloud, *Laplacian-based contraction* [73] is applied. Laplacian-based contraction minimizes the quadratic energy [73]:

$$\arg \min_{P'} \left(\|W_L L P'\|^2 + \sum_i W_{H,i}^2 \|p'_i - p_i\|^2 \right). \quad (2)$$

$P = \{p_i\}$ represents the original point cloud, $P' = \{p'_i\}$ the contracted point cloud, L is the Laplacian matrix, W_L the contraction weight matrix, and W_H the attraction weight matrix. The first term $\|W_L L P'\|^2$ represents the geometric details, which is subject to smoothing. The second term $\sum_i W_{H,i}^2 \|p'_i - p_i\|^2$ preserves the geometric shape of the point cloud. The contraction and the attraction weights balance the tendency to collapse into one point (“contraction”) and to remain at the current location (“attraction”). Equation 2 is solved in iterative fashion with increasing contraction weights and updated attraction weights which maintain shape and avoid full collapse.

The contracted point cloud lacks information about the connectivity of points. Thus, a *minimum spanning tree* is computed yielding a connected graph with all points under minimal edge lengths. The nodes of the spanning tree have degree of 1, 2, or more. Nodes of degree 1 are end nodes, nodes of degree 2 are intermediate nodes, and nodes of degree 3 or more are furcation nodes. The spanning tree is recursively partitioned at every furcation node to obtain unbranched polylines. Figure 2c displays the extracted medial axis (red) for the respective point cloud. The detected crack consists of 5 unbranched polylines. Figure 2d shows the medial axis overlaid on the textured mesh in 3D space.

7.3. Crack Width Estimation

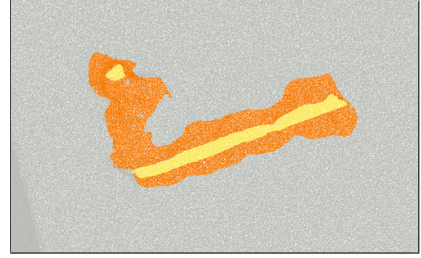
Once the 3D crack skeleton is extracted, the crack width can be estimated at individual points of the skeleton. For that purpose, the skeleton is sampled at regular intervals (e.g., 1 cm) and the given point is projected in all views. The single best view is selected according to a heuristic, which measures the angle between the viewing direction and point normal. From the given view, the intensity profile perpendicular to the propagation direction of the crack is extracted. The crack width can then be estimated by *rectangle transform* [74]: The approximately parabolic valley of the intensity profile is transformed into a rectangle of equal area yielding the estimated crack width. The chosen procedure is more robust towards image blur than other parabola-based methods.

7.3.1. Areal Defects

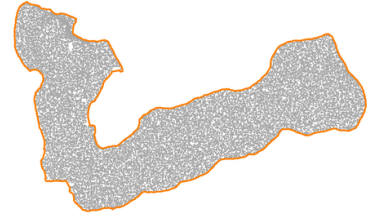
For areal defects such as spalling or corrosion skeletonization appears unsuited. Bounding boxes and convex hulls rather



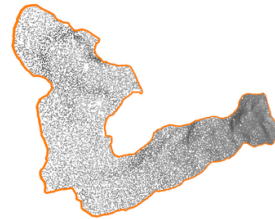
(a) Textured mesh showing an exposed reinforcement bar.



(b) Segmented point cloud with spalling and corrosion.



(c) Bounding polygon in 2D space.



(d) Bounding polygon transferred into 3D space.



(e) Bounding polygon on textured mesh in 3D space.

Figure 3: Illustration of the extraction of the bounding polygon for areal anomalies: (a) shows a textured mesh with spalling and corrosion, (b) the segmented point cloud, (c) the clustered point cloud (spalling and corrosion are merged to form one cluster) mapped on a 2D plane by means of PCA and the bounding polygon computed using alpha shapes, (d) the corresponding bounding polygon in 3D space, and (e) bounding polygon overlaid on the textured mesh.

coarsely outline the extension of an anomaly on the structure’s surface. Thus, to approximate the area covered by the anomaly, a *bounding polygon* is computed. For that purpose, the subcloud representing the instance of a spalling or corrosion is mapped into 2D space. This is accomplished by performing principal component analysis (PCA) on the subcloud and retaining only the two dimensions with most explanatory power of variance. These dimensions are supposed to represent the plane, in which the defect is located. Note that the procedure might fail for defects at corners, wall projections, and other non-planar conditions.

The polygon extraction in 2D space is performed by means of alpha shapes [75, 76]. Alpha shapes form a generalization of convex hulls and represent a bounding alpha hull, which encapsulates all respective points. The parameter α represents the radius $1/\alpha$ of a generalized disk and controls for the allowed concavity of the hull. For values α close to zero the alpha-hull approximates the common convex hull. For $\alpha < 0$ the alpha hull is defined as “the intersection of all closed complements of discs” [75] with radius $-1/\alpha$. With α approaching negative infinity the bounding hull with highest concavity is returned, which corresponds to the minimum spanning tree of the points.

This work uses the implementation of alpha complexes¹⁰ closely related to alpha shapes. Rather than arcs, alpha complexes compute an alpha hull consisting of straight lines derived from Delaunay triangulation. The choice of α depends on the density of the points and the scale of the space. In this work the PCA transformed points are in normalized space and an alpha value of $\alpha = 100$ rendered suitable. Figures 3a to 3e illustrate the bounding polygon for an exposed reinforcement bar. Figure 3a show the textured mesh of an exposed rebar, which in this work is modeled as the union of co-occurring spalling and corrosion. Figure 3b is a depiction of the segmented point cloud derived by the procedure described in Section 6. Orange refers to spalling and yellow to corrosion. Figure 3c displays the bounding polygon computed with alpha complexes in the 2D space. For that purpose, the 3D subcloud was mapped to 2D space by means of PCA. The vertices of the polygon in 2D space directly correspond to vertices in the 3D from which the 3D bounding polygon can be inferred, Figure 3d. Finally, the bounding 3D polygon can be displayed alongside the textured mesh, Figure 3e.

8. Results

After introducing the metrics for quantitative evaluation, this section presents quantitative and qualitative results of the proposed workflow.

8.1. Evaluation Metrics

The basic evaluation procedure for the quantitative evaluation corresponds to [77, 78, 79]. The vertices of both the medial axes and the bounding polygon are granted a positional tolerance τ based on the Euclidean distance measure d . The true

	Tol. [cm]	IoU [%]			AP ₅₀ [%]		
		Crack	Spall.	Corr.	Crack	Spall.	Corr.
<i>TopoCrack</i>	1.0	69.0	–	–	5.6	–	–
	2.0	72.7	–	–	9.1	–	–
	4.0	79.5	–	–	14.9	–	–
	6.0	83.3	–	–	17.4	–	–
	8.0	85.6	–	–	22.2	–	–
<i>nnU-Net</i>	1.0	66.0	10.8	35.1	8.6	3.2	36.8
	2.0	71.3	17.4	75.8	10.4	16.2	68.8
	4.0	78.9	27.6	96.9	17.5	47.6	73.3
	6.0	85.0	43.7	99.5	31.8	61.7	78.6
	8.0	90.6	55.3	100.0	44.8	72.0	78.6
<i>DetectionHMA</i>	1.0	89.0	15.8	17.0	22.3	16.0	11.6
	2.0	91.5	25.4	47.0	27.8	32.7	49.0
	4.0	94.9	40.5	81.5	45.0	44.5	55.6
	6.0	96.7	58.3	89.7	52.6	53.3	55.6
	8.0	99.0	77.2	95.8	62.5	64.0	64.1

Table 2: Quantitative test results for 3D damage detection. The approaches TopoCrack [1], nnU-Net [65], and DetectionHMA [3] are compared. IoU refers to the intersection-over-union for 3D semantic segmentation and AP₅₀ to the average precision (overlap 50% or more) for instance-level evaluation. “Tol.” refers to the positional tolerance granted.

positives (TP), the false negatives (FN), and the false positives (FP) are defined as:

$$TP(\tau) = \sum_{t \in \mathcal{T}} [d(t, p) \leq \tau] \quad (3)$$

$$FN(\tau) = \sum_{t \in \mathcal{T}} [\tau < d(t, p)] \quad (4)$$

$$FP(\tau) = \sum_{p \in \mathcal{P}} [\tau < d(t, p)] \quad (5)$$

where t denotes the true 3D vertices and p the predicted 3D vertices of the medial axis resp. the bounding polygon. The square brackets $[\cdot]$ refer to the Iverson brackets, which evaluate to one when the respective conditional is fulfilled, zero otherwise. The *intersection-over-union* is calculated by $\text{IoU}(\tau) = TP(\tau)/(TP(\tau) + FN(\tau) + FP(\tau))$.

In order to assess the instance detection capabilities of the proposed workflow, the standard metric *average precision* is used, which derives from the integral of the precision-recall curve. An overlap threshold of $\text{IoU}(\tau)$ of 50% is used; instances with more overlap are considered true positives, otherwise they form false positives or false negatives respectively. Analogously to IoU, AP₅₀(τ) is granted a positional tolerance represented by parameter τ .

¹⁰<https://github.com/bellockk/alphashape>

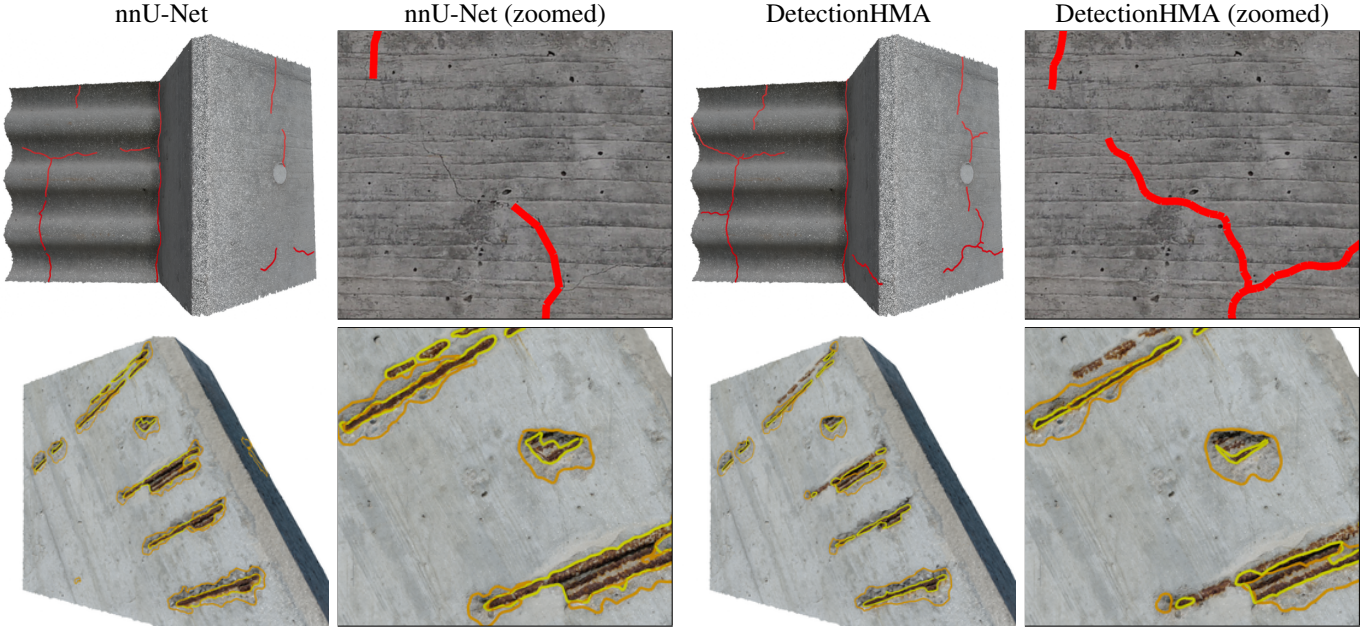


Figure 4: Qualitative test results for 3D damage detection. The top row shows the test segment of Bridge B, the bottom row shows the test segment of Bridge G. The results of nnU-Net [65] and DetectionHMA [3] are compared. While nnU-Net achieves better results for spalling and corrosion, DetectionHMA [3] shows more robust performance for crack detection. In zoomed view: medial axis and bounding polygons overlaid on textured mesh. Best viewed on screen.

8.2. Quantitative Results

Table 2 lists the quantitative results. It is observed, that TopoCrack performs decent in terms of IoU, while showing weaker performance in AP. The lower performance is likely due to the different dataset it was trained on: the TOPO dataset seems to represent a slightly different distribution than the S2DS dataset. The other two approaches are trained on the S2DS dataset. The TOPO dataset does not feature anomalies beyond cracks, therefore no results for spalling and corrosion are reported for TopoCrack.

DetectionHMA consistently outperforms the other two approaches for cracks detection. In terms of spalling, DetectionHMA takes the lead for IoU with nnU-Net, however, achieving higher AP for larger tolerances. Corrosion detection is best performed by nnU-Net over all levels of tolerance. The performance consistently and expectedly improves with increasing tolerance for all three approaches.

The good performance of nnU-Net for areal anomalies (spalling and corrosion) is especially insightful: its general purpose nature, which solely relies on self-configuration without manual intervention, achieves similar or better results than the DetectionHMA, which was specially fine-tuned on the domain dataset. However, nnU-Net lags behind in terms of crack detection. Apparently, concepts in medical imaging resemble areal objects rather than line-like objects in the few-pixels regime. This observation suggests further directions of research.

[3] argue that a positional tolerance of 4 cm can be considered a reasonable trade-off between positional accuracy and detection performance. Following this assumption, the mere numbers of IoU of over 90% for crack and corrosion form a powerful basis for effectively supporting structural inspection. Spalling appears to be the most challenging category with a top

performance of 77% at 8 cm tolerance. It is conjectured, that spalling is hard to detect from image features only and substantially benefits from true 3D detection.

The numbers in terms of instance detection are distinctly lower, which coincides with other literature: slight offsets and discontinuities in object instances quickly reduces the achieved AP. For more in-depth automated quantitative analysis, APs of 40% to 50% appear too low. To investigate the reasons and implications of the lower performance in AP and to improve the performance in instance detection render fruitful directions of future research.

8.3. Qualitative Results

Figure 4 shows the qualitative results on the test segments for Bridge B (top row) and G (bottom row). Based on the lower performance, the results of TopoCrack are not displayed. It tends to yield oversegmented cracks leading to a high number of false positives. While nnU-Net robustly detects the wider cracks, it misses to segment more narrow cracks and the narrowing spurs of cracks. In accordance with the quantitative results, DetectionHMA performs better capturing also the narrow (parts of) cracks. Unlike TopoCrack, nnU-Net and DetectionHMA tend to not oversegment cracks, leading to a low number of false positives. For practical applications, it might, however, be favorable to increase the sensitivity of the models – e.g., by down-weighting the predictions for background – in order to reduce the type II error. Thereby, the chance of missing crack is reduced at the cost of more false positives.

Based on the results for the test segment of Bridge G, Figure 4, bottom, the quantitative results for spalling and corrosion can be confirmed. nnU-Net achieves a robust detection of corrosion, while DetectionHMA seems to struggle with a number

of corrosion instances. For nnU-Net, the corrosion was more consistently segmented in the respective views, while DetectionHMA shows a more view-dependent segmentation performance. The inconsistency in image-level predictions for DetectionHMA was propagated into the mapping procedure, yielding a negative response for the respective points. A more sophisticated fusion procedure, which up-weights positive responses and/or takes the view properties into account, might have improved the results. To investigate and control the contribution of views forms an interesting direction for future research.

In terms of spalling detection, it is observed that DetectionHMA struggles for the lower spalling instance in the zoomed view, while nnU-Net manages to detect it successfully. While some fractions of a spalling instance are detected, both approaches regularly fail to segment the full extent of the spalling. Since spalling usually leaves a distinct 3D footprint, native 3D detection might benefit spalling detection as mentioned earlier.

9. Conclusion

Evidence was presented that the proposed workflow is a powerful tool for detecting structural anomalies in the 3D space. Based on the lack of available 3D data, leveraging the good performance of image-based models for anomaly segmentation forms a viable approach. The SOTA models of TopoCrack, nnU-Net, and DetectionHMA show a promising basis for multi-view anomaly detection. While TopoCrack tends to produce many false positives, DetectionHMA shows superior performance for cracks and nnU-Net performs favorably on areal anomalies such as spalling and corrosion. The segmentation performance partly achieves IoU of more than 90%. Instance segmentation measured in AP, however, is distinctly lower and currently not high enough for more advanced quantitative analyses.

Most work on anomaly detections stops after semantic segmentation. It is here emphasized, that only the knowledge about instances of anomalies enables further analytic processing in terms of their size and extent. For that purpose, robust procedures for the extraction of medial axes of cracks and bounding polygons of areal anomalies are proposed. Point cloud contraction yields the medial axis of a crack, from which the length and – with further processing – the width can be inferred. Using PCA and alpha shapes the bounding polygon of areal anomalies can be computed, enabling the estimation of the areal extend of the anomalies.

The general purpose, self-configuring approach of nnU-Net performed favorably on areal anomalies. It is, however, lagging behind the performance in crack segmentation of DetectionHMA, which was carefully fine-tuned on cracks and other anomalies represented in the S2DS dataset. Extending nnU-Net for fine structures such as cracks could pave the road to a general purpose approach to semantic segmentation of structural anomalies with minimal manual intervention.

Furthermore, the investigation, why the performance on instance-level is distinctly lower than the segmentation performance can lead to fruitful insights, which eventually lead to

improvements in instance-level detection. Forming a particularly challenging class, spalling detection can substantially benefit from exploring native 3D detection for structural anomalies. In terms of information transfer from 2D to 3D more sophisticated fusion schemes could compensate for false hits or misses in image-level segmentation.

During this work, one major drawback became apparent: the difficult scalability of point clouds. In real-world inspection scenarios, cracks of width 0.3 mm are relevant. In order to properly represent them, point clouds of very high density are required. Given the large areas, that need to be covered in bridges, these point clouds easily reach millions and billions of points. The current technology does not straightforwardly support the processing of such large point clouds. Thus, it must be investigated whether point clouds are a suited representation for real-world inspection scenarios. Conceptually, a bridge might more suitably be represented as a textured mesh: the texture can provide high visual resolution while the mesh represents a certain degree of geometric detail.

References

- [1] B. G. Pantoja-Rosero, D. Oner, M. Kozinski, R. Achanta, P. Fua, F. Pérez-Cruz, K. Beyer, Topo-loss for continuity-preserving crack detection using deep learning, *Construction and Building Materials* 344 (2022) 128264.
- [2] C. Benz, P. Debus, T. Gebhardt, E. Friedli, S. Schuhbäck, T. Zimmer, G. Morgenthal, V. Rodehorst, Ai-assisted inspection of concrete surfaces at dams, *avn-Allgemeine Vermessungs-Nachrichten* (6) (2023) 215–225.
- [3] C. Benz, V. Rodehorst, Image-based detection of structural defects using hierarchical multi-scale attention, in: *Pattern Recognition: 44th DAGM German Conference, DAGM GCPR 2022, Konstanz, Germany, September 27–30, 2022, Proceedings, Springer, 2022*, pp. 337–353.
- [4] A. Mohan, S. Poobal, Crack detection using image processing: A critical review and analysis, *Alexandria Engineering Journal* 57 (2) (2018) 787–798.
- [5] I. Abdel-Qader, O. Abudayyeh, M. E. Kelly, Analysis of edge-detection techniques for crack identification in bridges, *Journal of Computing in Civil Engineering* 17 (4) (2003) 255–263.
- [6] H. Oliveira, P. L. Correia, Automatic road crack detection and characterization, *IEEE Transactions on Intelligent Transportation Systems* 14 (1) (2012) 155–168.
- [7] A. M. A. Talab, Z. Huang, F. Xi, L. HaiMing, Detection crack in image using otsu method and multiple filtering in image processing techniques, *Optik* 127 (3) (2016) 1030–1033.
- [8] S. K. Sinha, P. W. Fieguth, Automated detection of cracks in buried concrete pipe images, *Automation in construction* 15 (1) (2006) 58–72.
- [9] M. Salman, S. Mathavan, K. Kamal, M. Rahman, Pavement crack detection using the gabor filter, in: *16th international IEEE conference on intelligent transportation systems (ITSC 2013)*, IEEE, 2013, pp. 2039–2044.
- [10] R. G. Lins, S. N. Givigi, Automatic crack detection and measurement based on image analysis, *IEEE Transactions on Instrumentation and Measurement* 65 (3) (2016) 583–590.
- [11] C. M. Yeum, S. J. Dyke, Vision-based automated crack detection for bridge inspection, *Computer-Aided Civil and Infrastructure Engineering* 30 (10) (2015) 759–770.
- [12] Q. Zou, Y. Cao, Q. Li, Q. Mao, S. Wang, Cracktree: Automatic crack detection from pavement images, *Pattern Recognition Letters* 33 (3) (2012) 227–238.
- [13] Y. Shi, L. Cui, Z. Qi, F. Meng, Z. Chen, Automatic road crack detection using random structured forests, *IEEE Transactions on Intelligent Transportation Systems* 17 (12) (2016) 3434–3445.
- [14] S. Dorafshan, R. J. Thomas, M. Maguire, Comparison of deep convolutional neural networks and edge detectors for image-based crack detection in concrete, *Construction and Building Materials* 186 (2018) 1031–1045.

- [15] A. Krizhevsky, I. Sutskever, G. E. Hinton, Imagenet classification with deep convolutional neural networks, *Advances in neural information processing systems* 25 (2012) 1097–1105.
- [16] S. Dorafshan, R. J. Thomas, M. Maguire, Sdnet2018: An annotated image dataset for non-contact concrete crack detection using deep convolutional neural networks, *Data in brief* 21 (2018) 1664–1668.
- [17] L. Zhang, F. Yang, Y. D. Zhang, Y. J. Zhu, Road crack detection using deep convolutional neural network, in: 2016 IEEE international conference on image processing (ICIP), IEEE, 2016, pp. 3708–3712.
- [18] F.-C. Chen, M. R. Jahanshahi, Nb-cnn: Deep learning-based crack detection using convolutional neural network and naïve bayes data fusion, *IEEE Transactions on Industrial Electronics* 65 (5) (2017) 4392–4400.
- [19] Y.-J. Cha, W. Choi, O. Büyüköztürk, Deep learning-based crack damage detection using convolutional neural networks, *Computer-Aided Civil and Infrastructure Engineering* 32 (5) (2017) 361–378.
- [20] X. Yang, H. Li, Y. Yu, X. Luo, T. Huang, X. Yang, Automatic pixel-level crack detection and measurement using fully convolutional network, *Computer-Aided Civil and Infrastructure Engineering* 33 (12) (2018) 1090–1109.
- [21] J. Long, E. Shelhamer, T. Darrell, Fully convolutional networks for semantic segmentation, in: *Proceedings of the IEEE conference on computer vision and pattern recognition*, 2015, pp. 3431–3440.
- [22] V. Badrinarayanan, A. Kendall, R. Cipolla, Segnet: A deep convolutional encoder-decoder architecture for image segmentation, *IEEE transactions on pattern analysis and machine intelligence* 39 (12) (2017) 2481–2495.
- [23] Q. Zou, Z. Zhang, Q. Li, X. Qi, Q. Wang, S. Wang, Deepcrack: Learning hierarchical convolutional features for crack detection, *IEEE Transactions on Image Processing* 28 (3) (2018) 1498–1512.
- [24] Y. Liu, J. Yao, X. Lu, R. Xie, L. Li, Deepcrack: A deep hierarchical feature learning architecture for crack segmentation, *Neurocomputing* 338 (2019) 139–153.
- [25] C.-Y. Lee, S. Xie, P. Gallagher, Z. Zhang, Z. Tu, Deeply-supervised nets, in: *Artificial intelligence and statistics*, Pmlr, 2015, pp. 562–570.
- [26] K. He, J. Sun, X. Tang, Guided image filtering, *IEEE transactions on pattern analysis and machine intelligence* 35 (6) (2012) 1397–1409.
- [27] S. Zheng, S. Jayasumana, B. Romera-Paredes, V. Vineet, Z. Su, D. Du, C. Huang, P. H. Torr, Conditional random fields as recurrent neural networks, in: *Proceedings of the IEEE international conference on computer vision*, 2015, pp. 1529–1537.
- [28] O. Ronneberger, P. Fischer, T. Brox, U-net: Convolutional networks for biomedical image segmentation, in: *International Conference on Medical Image Computing and Computer-assisted Intervention*, Springer, 2015, pp. 234–241.
- [29] T.-Y. Lin, P. Goyal, R. Girshick, K. He, P. Dollár, Focal loss for dense object detection, in: *Proceedings of the IEEE international conference on computer vision*, 2017, pp. 2980–2988.
- [30] Z. Liu, Y. Cao, Y. Wang, W. Wang, Computer vision-based concrete crack detection using u-net fully convolutional networks, *Automation in Construction* 104 (2019) 129–139.
- [31] F. Yang, L. Zhang, S. Yu, D. Prokhorov, X. Mei, H. Ling, Feature pyramid and hierarchical boosting network for pavement crack detection, *IEEE Transactions on Intelligent Transportation Systems* 21 (4) (2019) 1525–1535.
- [32] S. Xie, Z. Tu, Holistically-nested edge detection, in: *Proceedings of the IEEE international conference on computer vision*, 2015, pp. 1395–1403.
- [33] H. Liu, X. Miao, C. Mertz, C. Xu, H. Kong, Crackformer: Transformer network for fine-grained crack detection, in: *Proceedings of the IEEE/CVF International Conference on Computer Vision*, 2021, pp. 3783–3792.
- [34] K. Simonyan, A. Zisserman, Very deep convolutional networks for large-scale image recognition, *arXiv preprint arXiv:1409.1556* (2014).
- [35] A. Tao, K. Sapra, B. Catanzaro, Hierarchical multi-scale attention for semantic segmentation, *arXiv preprint arXiv:2005.10821* (2020).
- [36] Z. Chen, J. Zhang, Z. Lai, G. Zhu, Z. Liu, J. Chen, J. Li, The devil is in the crack orientation: A new perspective for crack detection, in: *Proceedings of the IEEE/CVF International Conference on Computer Vision*, 2023, pp. 6653–6663.
- [37] E. Bianchi, M. Hebbon, Development of extendable open-source structural inspection datasets, *Journal of Computing in Civil Engineering* 36 (6) (2022) 04022039.
- [38] S. Kulkarni, S. Singh, D. Balakrishnan, S. Sharma, S. Devunuri, S. C. R. Korlapati, Crackseg9k: A collection and benchmark for crack segmentation datasets and frameworks, *arXiv preprint arXiv:2208.13054* (2022).
- [39] L.-C. Chen, Y. Zhu, G. Papandreou, F. Schroff, H. Adam, Encoder-decoder with atrous separable convolution for semantic image segmentation, in: *Proceedings of the European conference on computer vision (ECCV)*, 2018, pp. 801–818.
- [40] M. Mundt, S. Majumder, S. Murali, P. Panetsos, V. Ramesh, Meta-learning convolutional neural architectures for multi-target concrete defect classification with the concrete defect bridge image dataset, in: *Proceedings of the IEEE/CVF Conference on Computer Vision and Pattern Recognition*, 2019, pp. 11196–11205.
- [41] P. Hühwohl, R. Lu, I. Brilakis, Multi-classifier for reinforced concrete bridge defects, *Automation in Construction* 105 (2019) 102824.
- [42] G. Huang, Z. Liu, L. Van Der Maaten, K. Q. Weinberger, Densely connected convolutional networks, in: *Proceedings of the IEEE conference on computer vision and pattern recognition*, 2017, pp. 4700–4708.
- [43] J. Flotzinger, P. J. Rösch, N. Oswald, T. Braml, Building inspection toolkit: Unified evaluation and strong baselines for damage recognition, *arXiv preprint arXiv:2202.07012* (2022).
- [44] E. Bianchi, M. Hebbon, Visual structural inspection datasets, *Automation in Construction* 139 (2022) 104299.
- [45] L. Yang, B. Li, W. Li, Z. Liu, G. Yang, J. Xiao, Deep concrete inspection using unmanned aerial vehicle towards cscs database, in: *Proceedings of the IEEE/RSJ international conference on intelligent robots and systems*, 2017, pp. 24–28.
- [46] Y. Bai, H. Sezen, A. Yilmaz, Detecting cracks and spalling automatically in extreme events by end-to-end deep learning frameworks, *ISPRS Annals of the Photogrammetry, Remote Sensing and Spatial Information Sciences* 2 (2021) 161–168.
- [47] J. Flotzinger, P. J. Rösch, T. Braml, dacl10k: Benchmark for semantic bridge damage segmentation, in: *Proceedings of the IEEE/CVF Winter Conference on Applications of Computer Vision*, 2024, pp. 8626–8635.
- [48] J. Flotzinger, P. J. Rösch, C. Benz, M. Ahmad, M. Cankaya, H. Mayer, V. Rodehorst, N. Oswald, T. Braml, Dacl-challenge: Semantic segmentation during visual bridge inspections, in: *Proceedings of the IEEE/CVF Winter Conference on Applications of Computer Vision*, 2024, pp. 716–725.
- [49] Z. Liu, H. Mao, C.-Y. Wu, C. Feichtenhofer, T. Darrell, S. Xie, A convnet for the 2020s, in: *Proceedings of the IEEE/CVF conference on computer vision and pattern recognition*, 2022, pp. 11976–11986.
- [50] Y. Fang, Q. Sun, X. Wang, T. Huang, X. Wang, Y. Cao, Eva-02: A visual representation for neon genesis, *arXiv preprint arXiv:2303.11331* (2023).
- [51] B. Cheng, I. Misra, A. G. Schwing, A. Kirillov, R. Girdhar, Masked-attention mask transformer for universal image segmentation, in: *Proceedings of the IEEE/CVF conference on computer vision and pattern recognition*, 2022, pp. 1290–1299.
- [52] P. Bergmann, X. Jin, D. Sattlegger, C. Steger, The mvtec 3d-ad dataset for unsupervised 3d anomaly detection and localization, *arXiv preprint arXiv:2112.09045* (2021).
- [53] P. Bergmann, D. Sattlegger, Anomaly detection in 3d point clouds using deep geometric descriptors, in: *Proceedings of the IEEE/CVF Winter Conference on Applications of Computer Vision*, 2023, pp. 2613–2623.
- [54] M. R. Jahanshahi, S. F. Masri, Adaptive vision-based crack detection using 3d scene reconstruction for condition assessment of structures, *Automation in Construction* 22 (2012) 567–576.
- [55] M. M. Torok, M. Golparvar-Fard, K. B. Kochersberger, Image-based automated 3d crack detection for post-disaster building assessment, *Journal of Computing in Civil Engineering* 28 (5) (2014) A4014004.
- [56] J. Huang, W. Liu, X. Sun, A pavement crack detection method combining 2d with 3d information based on Dempster-Shafer theory, *Computer-Aided Civil and Infrastructure Engineering* 29 (4) (2014) 299–313.
- [57] A. Zhang, K. C. Wang, B. Li, E. Yang, X. Dai, Y. Peng, Y. Fei, Y. Liu, J. Q. Li, C. Chen, Automated pixel-level pavement crack detection on 3d asphalt surfaces using a deep-learning network, *Computer-Aided Civil and Infrastructure Engineering* 32 (10) (2017) 805–819.
- [58] A. Zhang, K. C. Wang, Y. Fei, Y. Liu, S. Tao, C. Chen, J. Q. Li, B. Li, Deep learning-based fully automated pavement crack detection on 3d asphalt surfaces with an improved cracknet, *Journal of Computing in Civil Engineering* 32 (5) (2018) 04018041.
- [59] J. Chen, Y. K. Cho, Crackembed: Point feature embedding for crack segmentation from disaster site point clouds with anomaly detection, Ad-

- vanced Engineering Informatics 52 (2022) 101550.
- [60] B. G. Pantoja-Rosero, R. Achanta, K. Beyer, Damage-augmented digital twins towards the automated inspection of buildings, *Automation in Construction* 150 (2023) 104842.
 - [61] C. Steger, M. Ulrich, C. Wiedemann, *Machine vision algorithms and applications*, John Wiley & Sons, 2018.
 - [62] M. Pollefeys, L. Van Gool, M. Vergauwen, F. Verbiest, K. Cornelis, J. Tops, R. Koch, Visual modeling with a hand-held camera, *International Journal of Computer Vision* 59 (2004) 207–232.
 - [63] J. L. Schönberger, J.-M. Frahm, Structure-from-motion revisited, in: *Proceedings of the IEEE conference on computer vision and pattern recognition*, 2016, pp. 4104–4113.
 - [64] J. L. Schönberger, E. Zheng, J.-M. Frahm, M. Pollefeys, Pixelwise view selection for unstructured multi-view stereo, in: *Computer Vision—ECCV 2016: 14th European Conference, Amsterdam, The Netherlands, October 11–14, 2016, Proceedings, Part III 14*, Springer, 2016, pp. 501–518.
 - [65] F. Isensee, P. F. Jaeger, S. A. Kohl, J. Petersen, K. H. Maier-Hein, nnu-net: a self-configuring method for deep learning-based biomedical image segmentation, *Nature methods* 18 (2) (2021) 203–211.
 - [66] V. Iglovikov, A. Shvets, Ternaunet: U-net with vgg11 encoder pre-trained on imagenet for image segmentation, *arXiv preprint arXiv:1801.05746* (2018).
 - [67] D. Oner, M. Koziński, L. Citraro, N. C. Dadap, A. G. Konings, P. Fua, Promoting connectivity of network-like structures by enforcing region separation, *IEEE Transactions on Pattern Analysis and Machine Intelligence* 44 (9) (2021) 5401–5413.
 - [68] F. Isensee, C. Ulrich, T. Wald, K. H. Maier-Hein, Extending nnu-net is all you need, in: *BVM Workshop*, Springer, 2023, pp. 12–17.
 - [69] M. Cordts, M. Omran, S. Ramos, T. Rehfeld, M. Enzweiler, R. Benenson, U. Franke, S. Roth, B. Schiele, The cityscapes dataset for semantic urban scene understanding, in: *Proceedings of the IEEE conference on computer vision and pattern recognition*, 2016, pp. 3213–3223.
 - [70] Y. Yuan, X. Chen, J. Wang, Object-contextual representations for semantic segmentation, in: *ECCV 2020: 16th European Conference on Computer Vision, Glasgow, UK, August 23–28, 2020, Proceedings, Part VI 16*, Springer, 2020, pp. 173–190.
 - [71] S. Zhao, Y. Wang, Z. Yang, D. Cai, Region mutual information loss for semantic segmentation, *arXiv preprint arXiv:1910.12037* (2019).
 - [72] M. Ester, H.-P. Kriegel, J. Sander, X. Xu, et al., A density-based algorithm for discovering clusters in large spatial databases with noise., in: *kdd*, Vol. 96, 1996, pp. 226–231.
 - [73] J. Cao, A. Tagliasacchi, M. Olson, H. Zhang, Z. Su, Point cloud skeletons via laplacian based contraction, in: *Shape Modeling International Conference*, IEEE, 2010, pp. 187–197.
 - [74] C. Benz, V. Rodehorst, Model-based crack width estimation using rectangle transform, in: *17th International Conference on Machine Vision and Applications (MVA)*, IEEE, 2021, pp. 1–5.
 - [75] H. Edelsbrunner, D. Kirkpatrick, R. Seidel, On the shape of a set of points in the plane, *IEEE Transactions on information theory* 29 (4) (1983) 551–559.
 - [76] H. Edelsbrunner, E. P. Mücke, Three-dimensional alpha shapes, *ACM Transactions On Graphics (TOG)* 13 (1) (1994) 43–72.
 - [77] A. Knapitsch, J. Park, Q.-Y. Zhou, V. Koltun, Tanks and temples: Benchmarking large-scale scene reconstruction, *ACM Transactions on Graphics (ToG)* 36 (4) (2017) 1–13.
 - [78] N. Wang, Y. Zhang, Z. Li, Y. Fu, W. Liu, Y.-G. Jiang, Pixel2mesh: Generating 3d mesh models from single rgb images, in: *Proceedings of the European conference on computer vision (ECCV)*, 2018, pp. 52–67.
 - [79] G. Gkioxari, J. Malik, J. Johnson, Mesh r-cnn, in: *Proceedings of the IEEE/CVF international conference on computer vision*, 2019, pp. 9785–9795.